Optical Properties of Dispersed Aerosols in the Near Ultraviolet (355 nm): Measurement Approach and Initial Data

ARTICLE *in* ANALYTICAL CHEMISTRY · JUNE 2012

Impact Factor: 5.64 · DOI: 10.1021/ac3005814 · Source: PubMed

analytical chemistry

Article

pubs.acs.org/ac

Optical Properties of Dispersed Aerosols in the Near Ultraviolet (355 nm): Measurement Approach and Initial Data

Lulu Ma and Jonathan E. Thompson*

Department of Chemistry & Biochemistry, MS1061, Texas Tech University, Lubbock, Texas 79409, United States

Supporting Information

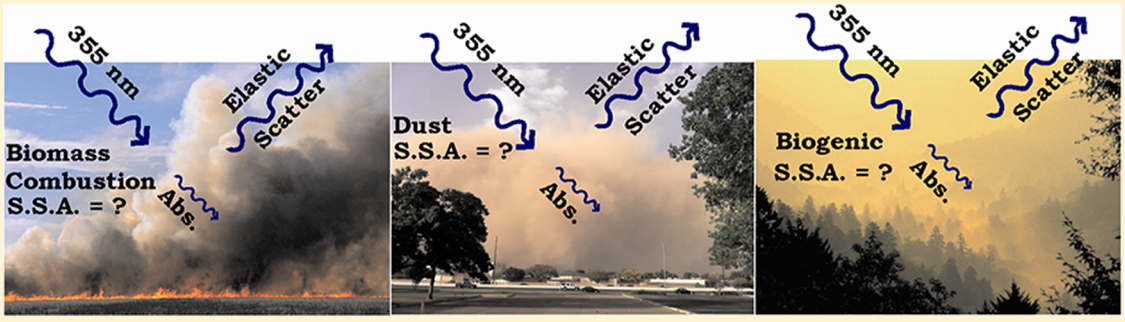

ABSTRACT: An aerosol albedometer combining cavity ring-down spectroscopy (CRDS) with integrating sphere nephelometry was developed for use at λ = 355 nm. The instrument measures extinction and scattering coefficients of dispersed particulate matter in the near ultraviolet (UV) spectral region. Several samples have been analyzed, including: ammonium sulfate, secondary organic aerosols (SOA) resulting from the ozonolysis of α-pinene and photooxidation of toluene, redispersed soil dust samples, biomass burning aerosols, and ambient aerosols. When particle size and number density were experimentally controlled, extinction coefficients and scattering coefficients were found to have a linear relationship with particle number concentration, in good agreement with light scattering theory. For ammonium sulfate and pinene samples, extinction cross sections for size-selected (D_p = 300 nm) samples were within the range of 1.65−2.60 × 10^{-9} cm^2 with the largest value corresponding to ammonium sulfate and the lowest value for pinene SOA. The scattering cross sections of pinene and ammonium sulfate aerosols were indistinguishable from the extinction cross sections, indicating that these particle types had minimal light absorption at 355 nm. However, soil dusts and biomass burning aerosols showed significant absorption with single scatter albedo (SSA) between 0.74 and 0.84. Ambient aerosols also had transient absorption at 355 nm that correlated well with a particle-soot absorption photometer (PSAP) measuring visible light absorption.

Fine solid and liquid particles suspended in the atmosphere (aerosols) scatter and absorb solar radiation, and this causes a climate effect that is often quantitatively estimated by the aerosol's "direct radiative forcing" (RF).[1,2] Compared to well-mixed greenhouse gases that absorb long-wave radiation, aerosols have influence mainly on short-wave radiation with a total direct RF of approximately −0.5 $W \cdot m^{-2}$.[1−3] A positive RF indicates a heating influence, while a negative RF suggests a cooling influence.

Light scattering, absorption, and extinction coefficients (b_{scat}, b_{abs}, b_{ext}; m^{-1}) are the quantitative variables often used to describe these differing effects. The extinction coefficient (b_{ext}) is the sum of the effects of absorption and scattering (see eq 1) and is defined through eq 2.

$$b_{ext} = b_{scat} + b_{abs} \quad (1)$$

$$I_z = I_0 e^{-(b_{ext} z)} \quad (2)$$

In eq 2, I_z, and I_0 are irradiances at point z meters and at z = 0 m, respectively. Light scattering leads to a cooling of climate, while strong absorption can lead to a warming. The interplay between scattering and absorption can be described through the aerosol single scatter albedo (SSA, unitless) defined as:

$$\omega = \frac{b_{scat}}{b_{ext}} \quad (3)$$

For those aerosols that have no absorption, extinction of light is only composed of scattering, and SSA equals one. If light is absorbed, SSA will fall below one.

In this work, the optical properties of aerosols are studied by combining cavity ring-down spectroscopy (CRDS)[4−8] and integrating sphere nephelometry. The innovative aspect of this project is the use of a pulsed Nd:YAG laser at λ = 355 nm as a light source to access the near ultraviolet (UV) region. The literature record consists of many papers that study the optical properties of aerosols in the visible spectral range; however, there are far fewer studies in the near UV. Of available data, many studies involve column integrated inversions of direct and

Received: March 1, 2012
Accepted: June 8, 2012
Published: June 8, 2012

   dx.doi.org/10.1021/ac3005814 | *Anal. Chem.* 2012, 84, 5611−5617

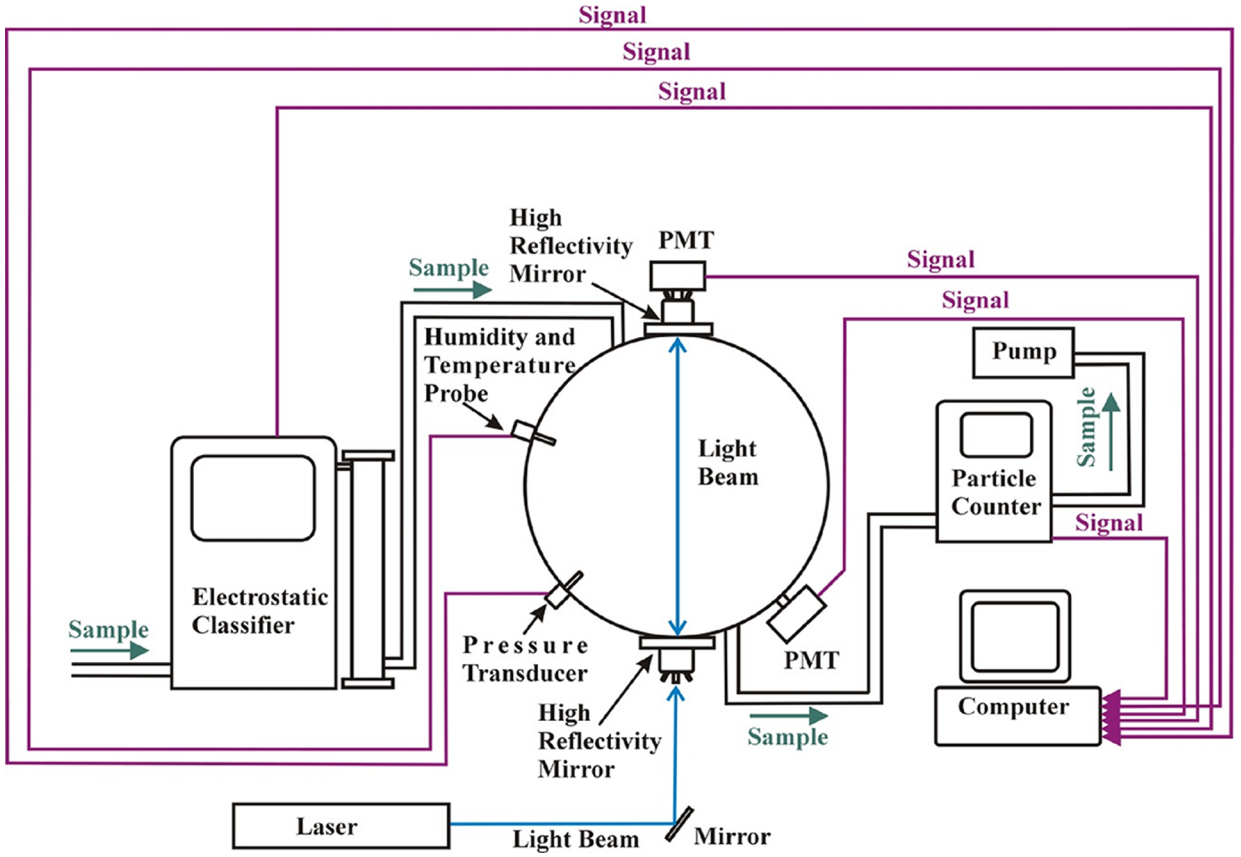

Figure 1. Schematic of the measurement apparatus. The electrostatic classifier was used to select 300 nm diameter particles for $(NH_4)_2SO_4$ and SOA experiments but removed for experiments on dust, ambient aerosol, and biomass burning aerosols. The 3rd harmonic of a Nd:YAG laser was used to produce 5 ns pulses at λ = 355 nm.

diffuse sky radiances from radiometer and/or sun-photometer data. A recent example of this is found in Corr et al.[9] These authors estimate near UV SSA in the vicinity of 0.8 for the Mexico City metropolitan area and also present a summary of additional inversions presented in the literature for a variety of global locations with resulting SSA values ranging from 0.65 to nearly 1.0 for the 300−400 nm spectral window. Unfortunately, extracting aerosol optical data through these inversion methods can be prone to difficulties due to variable light absorption by atmospheric gases aloft and poorly constrained surface reflectivity estimates in the UV. The latter alters actinic flux and consequently the observed radiances. In addition, the process is time-consuming, and measurements can only be made during the day and in the absence of cloud cover.

UV light is known to play a very important role in tropospheric photochemistry, and significant recent evidence suggests that a class of material present in atmospheric particulate matter (commonly called "brown-carbon") absorbs light strongly in the near UV spectral window.[10−14] The potential impact of this material on atmospheric radiative transport and photochemistry makes the development of techniques for single-point measurement of light scattering and absorption between 290 and 400 nm a research priority for the atmospheric chemistry community. In addition, active, single point measurements of aerosol optics offer the ability to manipulate the aerosol sample chemically or physically prior to measurement. For instance, thermo-denuders can be used to remove volatile material, or the effect of relative humidity on optical signatures can be studied. This simply cannot be accomplished using columnar inversions. At present, it appears that only photoacoustic spectroscopy has been employed to make point measurements of aerosol absorption in the UV spectral window.[15,16] This manuscript documents an alternative measurement instrument and reports initial optical data for several types of common aerosols for the near UV (355 nm). It is envisioned that the measurement method and resulting data will assist in improving models of radiative transport in atmosphere.

■ OVERVIEW OF EXPERIMENTAL METHODS

Figure 1 is a schematic of the instrument setup. The apparatus used is very similar to that reported in Thompson et al.[17,18] with the major exception of the different measurement wavelength. To summarize the experimental work, the instrument sensitivity and precision has been evaluated through a series of experiments using filtered air and R-134a gas (tetraflouroethane). We find limits of detection for b_{scat}, b_{ext}, and b_{abs} of 12, 11, and 16 Mm^{-1}, respectively, for a 52 s integration time. In addition, optical measurements were made on size-selected 300 nm diameter (D_p) ammonium sulfate and pinene aerosols. Additional measurements were made on redispersed soil-dust proxies, toluene secondary organic aerosols (SOA), and biomass burning samples. Measurements on ambient aerosols have also been made with the device, and these were compared to measurements made simultaneously with commercial products. Details of particle generation, dust size distribution, data treatment, and optical measurements are reported in the Supporting Information.

RESULTS AND DISCUSSION

Calibration Gas Experiments. Figure 2A illustrates the results of an experiment in which the measurement cell was

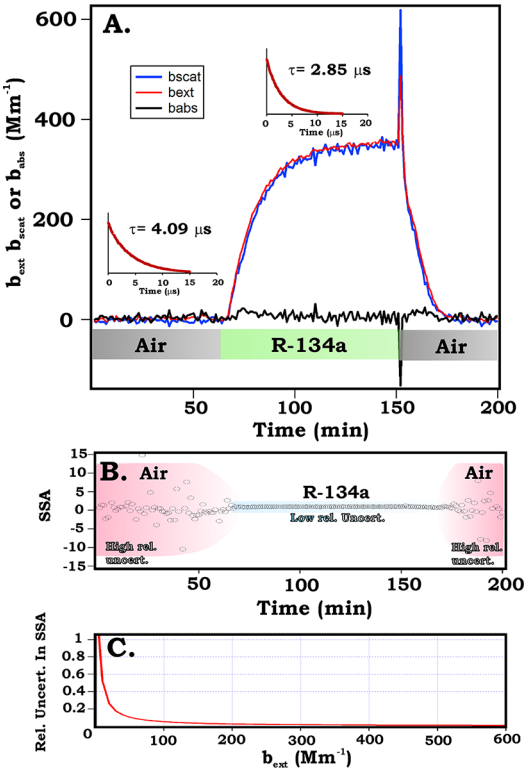

Figure 2. (A) Plots of observed scattering, extinction, and absorption coefficient in time for an experiment in which the cell was flushed sequentially with filtered air, R-134a, and air again. Insets show CRDS traces for air and R-134a demonstrating a shift in ring-down time constant (τ). In plot B, the SSA is plotted for the data from (A). Point to point measurements of SSA are highly variable when b_{scat} and b_{ext} are near zero, but much better precision is achieved for R-134a with $b_{ext} = b_{scat} \approx 370$ Mm^{-1}. This is consistent with the relative uncertainty in SSA propagated from observed standard deviations as shown in plot (C).

sequentially filled with filtered air, R-134a, and then filtered air. First, when only filtered room air was present, both extinction and scattering coefficients were zero. Then, both measurements approached 370 Mm^{-1} when the sphere was filled by R-134a. When the refrigerant gas was substituted by filtered room air again, the signals rapidly dropped back to zero. The measured absorption coefficient was zero during the entire experiment owing to the nonabsorptive nature of the gases. The spike in the data is an artifact that occurs when the refractive index (R.I.) of the gas within the cell changes very rapidly. It is believed this is due to a refractive effect at the interface between gases that are not yet well-mixed in the measurement cell. This experiment demonstrates monitoring changes in optical properties at λ = 355 nm is possible with the apparatus. Time resolution was limited by the washing out time of the 50 L sphere and varied between 20 and 40 min in this experiment depending on gas flow rate. The standard deviation of replicate filtered air measurements for b_{scat} was 3.9 Mm^{-1} and 3.5 Mm^{-1} for b_{ext}, and we are able to report 3σ limits of detection of 12 and 11 Mm^{-1} accordingly (52 s integration time). This is roughly 1 order of magnitude poorer performance than what our previous instrument at λ = 532 nm was able to achieve.[17] The cause of this is the poorer mirror reflectivity of UV optics compared to the visible. This decreases the effective sample path length for the experiment and reduces ring-down times, which increases relative error given a fixed imprecision in determining the ring-down constant, τ. Absorption is measured by the difference between b_{ext} and b_{scat}. As such, we can propagate standard deviation to b_{abs} using the standard approach,[19] and the result is 5.2 Mm^{-1}. This is in good agreement with the standard deviation of b_{abs} observations for zero air in Figure 2A. The limit of detection for b_{abs} (3σ) for single point measurements is therefore 16 Mm^{-1} at 355 nm. Figure 2B,C also illustrates how the variability in measured single scatter albedo (SSA) scales with the magnitude of extinction/scatter coefficient. Figure 2B is a plot of reported SSA in time as air is switched to R-134a (same X axis as in Figure 2A). As observed, when b_{ext} is near zero, SSA is highly variable but when b_{ext} increases, the precision of the SSA measurement improves significantly. This is a consequence of the SSA being a ratio of two measured values, each with its own imprecision. Propagation of relative uncertainty to SSA from the std. dev. of replicate b_{scat} and b_{ext} measurements yields the plot shown in Figure 2C, which suggests $b_{ext} \geq 60$ Mm^{-1} is required to achieve <10% relative uncertainty for single point measurements of SSA.

Size-Selected Ammonium Sulfate Aerosols and Secondary Organic Aerosol (SOA). Figure 3 and Table 1

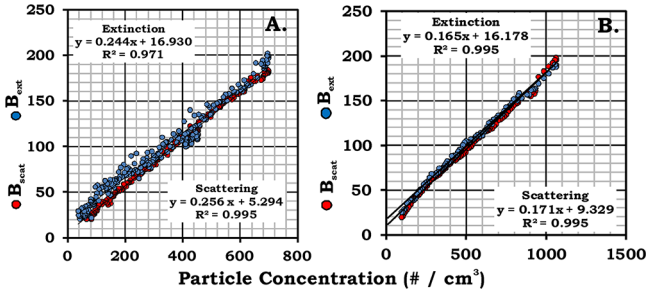

Figure 3. Plots of extinction and scattering coefficients at 355 nm vs particle concentration for lab generated (A) ammonium sulfate aerosols and (B) α-pinene SOA. Y-axis units are Mm^{-1}.

report results of experiments on size selected ammonium sulfate and secondary organic aerosol (SOA) produced from oxidation of α-pinene with ozone. A linear relationship between particle concentration and extinction coefficient is found in each measurement. Extinction cross sections (slope of the resulting lines) of D_p = 300 nm ammonium sulfate and pinene SOA were 2.4 ($\pm$0.8) $\times$ 10^{-9} cm^2 and 1.65 ($\pm$0.14) $\times$ 10^{-9} cm^2, respectively. Linear relationships were also found between particle concentration and scattering coefficient. The corresponding scattering cross sections are 2.6 ($\pm$1) $\times$ 10^{-9}cm^2 and 1.71 ($\pm$0.09) $\times$ 10^{-9} cm^2. Since the measured scattering cross sections for ammonium sulfate and pinene are statistically indistinguishable, no light absorption at λ = 355 was observed for these particle types.

In these experiments, the highest particle concentration was about 10^{3}cm^{-3} and particles with 300 nm diameter were selected with an electrostatic classifier, so aerosol particles are far away from each other inside the sphere and refractive index can be calculated from Mie theory via a method previously described.[20] One known caveat to the size selection process is

dx.doi.org/10.1021/ac3005814 | Anal. Chem. 2012, 84, 5611−5617

Table 1. Summary of Data and Extracted Refractive Indices for D_p = 300 nm Particles after Correction for Multiply Charged Particles

aerosol type	σ_{ext} ± 95% c.i. (× 10^{-9} cm^2)	σ_{scat} ± 95% c.i. (× 10^{-9} cm^2)	Measured R.I.	Literature R.I.
ammonium sulfate	2.4 ± 0.8	2.6 ± 1	1.56 ± 0.12	approx. 1.55 (ref 21)
pinene SOA	1.65 ± 0.14	1.71 ± 0.09	1.45 ± 0.02	1.46 ± 0.02 (ref 22)

multiply charged particles of differing diameter making it through the size selection process and being measured. We have corrected the optical measurements for this effect when necessary (determined to be approximately 5% of optical signal for ammonium sulfate and <1% for pinene). Table 1 lists scattering and extinction cross sections observed and extracted refractive indices. Cross section uncertainties reported are 95% confidence intervals. For refractive indices, uncertainty is governed by the approximate range of possible R.I. values that are bounded by the confidence intervals for the cross sections. As observed, best-fit refractive indices were 1.45 for pinene and 1.56 for ammonium sulfate. The refractive indices of ammonium sulfate and pinene SOA obtained from these measurements are very similar to values reported previously by Toon et al. and Nakayama et al. for 355 nm.[21,22]

Soil Dusts and Biomass Burning Aerosols. Table 2 lists SSA values of soil dusts, biomass burning aerosol, and toluene SOA. The dust and smoke have SSA well below one, indicating that they absorb light at 355 nm. For soil dust and biomass burning aerosols, no size selection was used and the particles were likely not spherical so absolute cross sections cannot be determined. Pullman and Amarillo soil dusts are native to the West Texas Panhandle and regional dust storms commonly aerosolize these materials. Additionally, both soil dust and biomass burning aerosols have large global source strengths, and knowledge of typical SSA values is of scientific significance. Both biomass combustion aerosol samples had similar SSA of 0.83−0.84. This value is in reasonably good agreement with that expected from extrapolation of the data of Dubovik et al. for authentic atmospheric smoke aerosols.[23] However, the combustion conditions (flaming vs smoldering) are known to significantly affect soot production and therefore alter SSA. In this work, we took no controls to ensure either flaming or smoldering conditions, and both were present during the experiment. For the soil dusts, Amarillo soil appeared to be significantly more light absorbing compared to Pullman. This is consistent with previous results on these soil samples observed for the visible region.[24] In addition, the SSA values reported here for the soil dusts at 355 nm are in good agreement with values expected from extrapolation of spectral trends previously presented in the literature.[25,26] For the toluene SOA experiments, size selection was used, but we were unable to produce an aerosol of sufficient monodispersity to extract refractive index values. It is believed that 300 nm particles were by far the most abundant in the sample, but a sufficient number of approximately 500 nm diameter particles were present to increase the optical signals by an expected value of 10−20%. The mean SSA of the toluene aerosol mixture observed was 0.95 ± 0.03 (mean ±95% conf. int.). Nakayama et al. have recently reported that toluene SOA absorbs light at 355 nm (SSA of approximately 0.83 from their data).[22] It is well-known that nitrated aromatics expected to be present in the toluene SOA at high NOx absorb light in the near UV and visible region.[27,28] The exact reason strong light absorption was not observed for toluene SOA in this experiment is unclear but is likely related to differences in reaction conditions between experiments.

Table 2. Near UV Single Scatter Albedo (SSA) of Biomass Burning, Soil-Dust, and Organic Aerosols[a]

		SSA ± 95% c.i.	measurement range (Mm^{-1})
SOA	toluene SOA	0.95 ± 0.03	20−200
soil dusts	pullman soil	0.84 ± 0.01	76−571
	amarillo soil	0.75 ± 0.01	120−530
biomass burning aerosols	pear tree leaves	0.84 ± 0.01	150−1390
	Afghanistan pine needle	0.83 ± 0.01	43−1386

[a]Additional data is presented in Supporting Information, Figure S-2.

Ambient Measurements. Ambient samples were also measured during the course of our investigations. Aerosol samples were pulled into the sphere directly from outside a laboratory window. Absorption coefficients at 355 nm were obtained by subtracting scattering coefficient (b_{scat}) from extinction coefficient (b_{ext}). In addition, simultaneous measure-

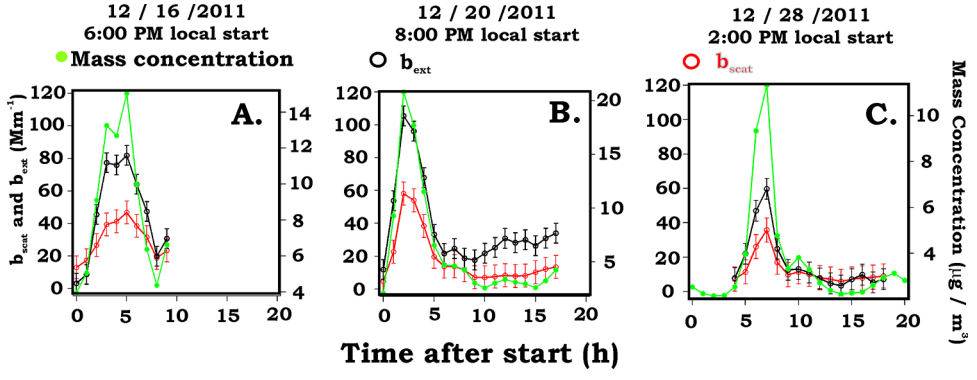

Figure 4. Plots of extinction and scattering coefficients (Mm^{-1}) and mass concentrations ($\mu g/m^3$) vs time for 3 aerosol plumes observed in Lubbock, TX. Plume A occurred on 12/16/2011, plume B on 12/20/2011, and plume C on 12/28/2011. For all ambient trials, sample $T \approx 301$ K, R.H. = 10−12%, and P = 0.88−0.90 atm. The consant error bars are set to the observed precision of the scatter and extinction channel.

dx.doi.org/10.1021/ac3005814 | Anal. Chem. 2012, 84, 5611−5617

ments of aerosol absorption coefficient at visible wavelengths and aerosol mass concentrations were recorded using a particle-soot absorption photometer (PSAP) and real time aerosol mass concentration monitor. Figure 4 is a comparison of the optical results from the albedometer and the aerosol mass monitor. The left Y-axis of Figure 4 is extinction (black) and scattering (red) coefficients (Mm^{-1}) of ambient aerosols. The Y-axis on the right plots the mass concentrations (green, $\mu g/m^3$) measured simultaneously. For these ambient trials, the sample temperature was consistently ≈301 K and the aerosol sample was dry with a relative humidity of only 10−12%. The average SSA at 355 nm during the Dec 16 plume was 0.55; the Dec 20 plume yielded a mean of 0.57, and the Dec 27 plume had a mean of 0.61. This is much lower than the values of 0.83−0.87 reported by Gyawali et al. for winter-time ambient aerosol in Reno, NV.[15] However, these authors did note the SSA tended to be lower during pollution plumes, so it is conceivable that our observations were made on discrete pollution plumes. In addition, measurements were made in winter during times of colder temperatures so smoke plumes from heating may influence the air sample. When comparing the mass concentration with extinction and scattering traces, we see both tend to track together in time. The magnitude of the measured values also suggest the atmospheric environment of Lubbock was clean as mass concentrations of ambient aerosols are often only a few $\mu g/m^3$. The relationship between mass concentration and optical effects can be better observed in Figure 5, as plots of b_{scat} and b_{ext} vs particle mass concentration

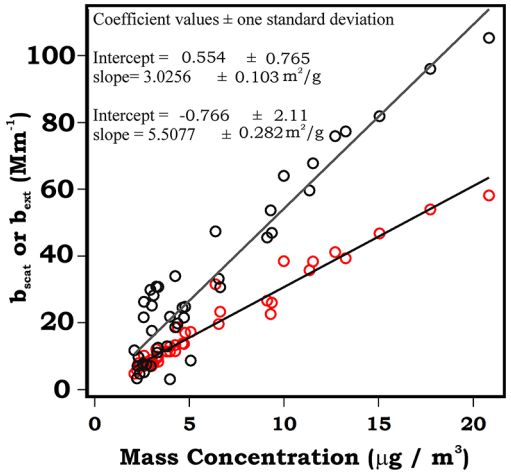

Figure 5. Plot of extinction (black) and scattering (red) coefficient vs mass concentration for ambient aerosol plumes in Lubbock, TX at 355 nm. The slopes of the lines are the mass scatter and mass extinction efficiencies, here 3.0 and 5.5 m^2/g.

have been presented. An approximate linear relationship between the variables is observed, and best-fit lines for both data sets have been included. The size distribution of particles influences the slope of the line, so there is no fundamental reason or assurance this plot should be linear. In fact, it will only be linear if the ambient particle size distribution is relatively constant. Nonetheless, the data analysis is useful as it relates optical effects directly to mass concentration of aerosol. The slope of the lines for scattering and extinction data were 3.0 and 5.5 m^2/g, respectively, for this data set. This data is based on 3 plumes of aerosols studied over a short period of time, during low aerosol mass loading, and likely does not represent the typical case for Lubbock, TX.

Figure 6 plots absorption coefficients (Mm^{-1}) at different wavelengths in time for the aerosol plumes previously mentioned. Absorption coefficients at 355 nm were obtained from the albedometer, and the visible wavelengths (470, 552, 660 nm) were obtained using the PSAP. Operational conditions for the PSAP are described in Supporting Information. The insets to the figure also show wind direction and speed along with aerosol Angstrom absorption exponent (AAE). AAE describes the wavelength dependence of light absorption by aerosol and was determined by fitting the PSAP data to a power law of the following form and extracting the exponent:

$$b_{abs} = k\lambda^{-(AAE)} \quad (4)$$

Larger AAE values indicate strong enhancement in light absorption at higher frequencies or shorter wavelengths. A quick glance at Figure 6 suggests b_{abs} values measured at different wavelengths by different techniques tend to track one-another in time. More careful consideration of Figure 6 yields the insight that a change in b_{abs} is often accompanied by a shift in AAE, but AAE can shift to either higher or lower values during a plume. This is particularly evident for the trace of December 28 when AAE dipped from 1.2 to <0.8 during the plume episode. However, on December 16 and December 20, larger AAE values were encountered during the plume. This is consistent with the magnitude of absorption at λ = 355 nm reflected in the data. For instance, in the plot for Dec 28, the b_{abs} value for 355 nm is very close to that observed for 470 nm indicating there was not a strong wavelength dependence on absorption. However, during the Dec 16 and Dec 20 plumes, the observed near UV aerosol absorption was significantly higher than that observed by the PSAP at 470 nm. This is consistent with the increase in the AAE measured via the PSAP measurements during the plume. Inclusion of the albedometer b_{abs} data at 355 nm in the AAE calculation significantly changes the AAE value. For instance, for the plumes of Dec 16 and Dec 20, AAE during the plume increases to 2.03 and 2.01 if 355 nm data is included. For the Dec 28 aerosol plume, an AAE of 0.61 would be obtained which is similar to that obtained from the PSAP alone. The phenomenon of apparent increases in AAE relative to filter based measurement techniques has also recently been reported by Ajtai et al. when those authors compared photoacoustic absorption measurements to those made simultaneously with an aethalometer.[29] A quick glance at Figure 6 is also enough to suggest the precision for the b_{abs} measurement afforded by the PSAP is superior to the albedometer difference measurement. The PSAP LOD for b_{abs} at visible wavelengths is <1 Mm^{-1} which is considerably better than what the difference method (albedometer) can offer in the UV. Literature reported limits of detection (LOD) for photoacoustic sensing of aerosol b_{abs} are also often <1Mm^{-1} in the visible region, but far less work has been reported in the UV region.[30] However, there are some reports to provide a comparison. Ajtai et al. have recently reported a UV version of a photoacoustic instrument to measure aerosol absorption with LODs of 3.5 and 6.7 Mm^{-1} at 355 and 266 nm.[29] Gyawali et al. have reported minimum detectable absorptions of <0.5 Mm^{-1} at 355 nm.[15] These data suggest the photoacoustic method offers improved sensitivity relative to the albedometer for absorption measurements in the UV. In addition, any small

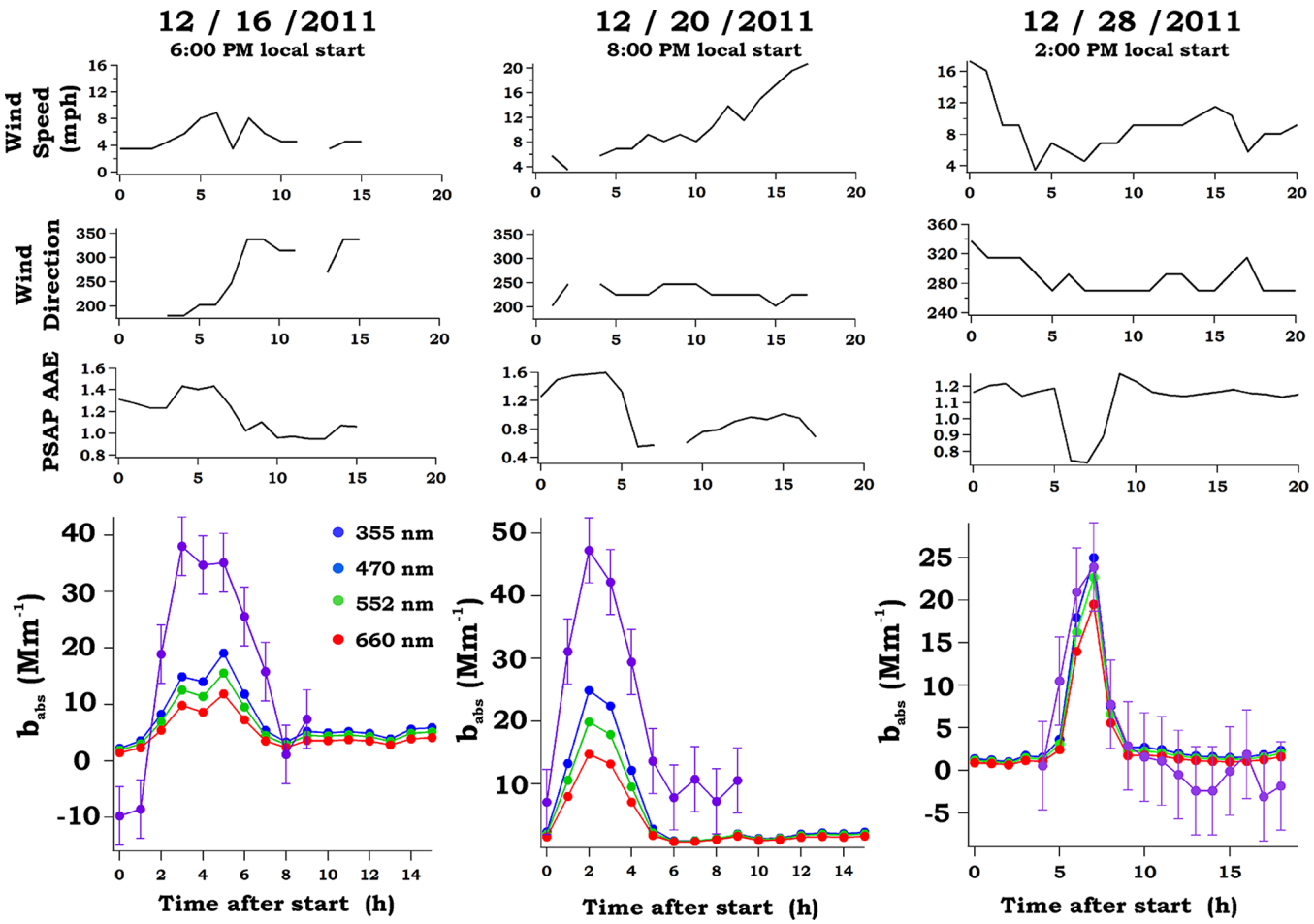

Figure 6. Plots of absorption coefficients (b_{abs}, Mm^{-1}) at different wavelengths (355, 470, 552, and 660 nm) vs time for three aerosol plumes observed at Lubbock, TX. The insets above the colored plots illustrate wind speed, wind direction, and Angstom absorption exponent (AAE) of the aerosol as measured from the PSAP. The constant error bars for the 355 nm trace are set to 5.2 Mm^{-1}, the propagated precision of the albedometer b_{abs} channel. Missing points for the wind data plots correspond to "calm" conditions.

signal drift in the extinction or scatter channel can lead to a large relative error in b_{abs}. This was frequently encountered and necessitated regular calibration which disrupted monitoring efforts. Alternatively, the PSAP (and most photoacoustic instruments) currently do not make measurements in the UV, and these techniques do not measure scattering or extinction. The albedometer b_{abs} measurement can provide some insight into ambient aerosol absorption, albeit not at the level of precision other techniques may offer. Therefore, the techniques are quite complementary, and the albedometer absorption measurement is best-suited for relatively polluted air masses.

CONCLUSIONS

A method for measuring aerosol scattering, extinction, absorption coefficients, and single scatter albedo in the near UV spectral region (355 nm) has been described. The optical properties of atmospheric aerosols in the near UV have not been explored to a large extent, and measurement instruments like the albedometer presented here have utility for making point measurements of aerosols. Results suggest that ammonium sulfate and an organic aerosol produced through the ozonolysis of α-pinene do not absorb light at 355 nm (e.g., SSA $\approx$ 1). However, data supports the conclusion aerosol produced from toluene vapor at low concentrations of NO_2 (<150 ppbv) may weakly absorb light at 355 nm (SSA = 0.95). Single scatter albedo values for biomass burning samples (SSA = 0.83−0.84) and windblown mineral dust (SSA = 0.75−0.84) have been reported for λ = 355 nm. These aerosol types are major constituents of authentic atmospheric aerosols, so data on their optical properties is relevant. In addition, the albedometer can be used for ambient aerosol measurements, and study of ambient plumes at our location has allowed extraction of limited data for near UV mass scatter (3.0 m^2 g^{-1}) and mass extinction efficiencies (5.5 m^2 g^{-1}). Also, the albedometer derived absorption measurement tracked simultaneous measurements made in the visible spectrum via a filter based PSAP instrument.

ASSOCIATED CONTENT

Supporting Information

Additional information as noted in text. This material is available free of charge via the Internet at http://pubs.acs.org.

AUTHOR INFORMATION

Corresponding Author

*E-mail: jon.thompson@ttu.edu. Phone: (806)742-3210.

Notes

The authors declare no competing financial interest.

■ ACKNOWLEDGMENTS

L.M. performed experiments, collected data, reported data, and assisted in authoring the manuscript. J.T. contributed to plotting data, providing guidance, and authoring/editing the manuscript. This research has been supported by the National Science Foundation (NSF) via grants ATM 0634872 and ATM 1004114 and by Texas Tech University/the State of Texas. The dust storm TOC graphic is courtesy of John Holsenbeck, National Weather Service, Lubbock, Texas.

■ REFERENCES

(1) Ramaswamy, V., et al. Radiative forcing of climate change. In *Climate Change 2001: The Scientific Basis. Contribution of Working Group I to the Third Assessment Report of the Intergovernmental Panel on Climate Change*; Houghton, J. T., Ding, Y., Griggs, D. J., Noguer, M., van der Linden, P. J., Dai, X., Maskell, K., Johnson, C. A., Eds; Cambridge University Press: Cambridge, UK, 2001.

(2) IPCC. *Climate Change 2007: The Physical Science Basis. Contribution of Working Group I to the Fourth Assessment Report of the Intergovernmental Panel on Climate Change*; Solomon, S., Qin, D., Manning, M., Chen, Z., Marquis, M., Averyt, K. B., Tignor, M., Miller, H. L., Eds.; Cambridge University Press: Cambridge, UK and New York, NY, USA, 2007.

(3) Ramanathan, V.; Crutzen, P. J.; Kiehl, J. T.; Rosenfeld, D. *Science* **2001**, *294*, 2119−2124.

(4) Bulatov, V.; Fisher, M.; Schechter, I. *Anal. Chim. Acta* **2002**, *466*, 1−9.

(5) Lang-Yona, N.; Rudich, Y.; Segre, E.; Dinar, E.; Abo-Riziq, A. *Anal. Chem.* **2009**, *81*, 1762−1769.

(6) Brown, S. S.; Stark, H.; Chicora, S. J.; McLaughlin, R. J.; Ravishankara, A. R. *Rev. Sci. Instrum.* **2002**, *73*, 3291−3301.

(7) Thompson, J. E.; Smith, B. W.; Winefordner, J. D. *Anal. Chem.* **2002**, *74*, 1962−1967.

(8) Thompson, J. E.; Nasajpour, H. D.; Smith, B. W.; Winefordner, J. D. *Aerosol Sci. Technol.* **2003**, *37*, 221−230.

(9) Corr, C. A.; Krotkov, N.; Madronich, S.; Slusser, J. R.; Holben, B.; Gao, W.; Flynn, J.; Lefer, B.; Kreidenweis, S. M. *Atmos. Chem. Phys.* **2009**, *9*, 5813−5827.

(10) Alexander, D. T. L.; Crozier, P. A.; Anderson, J. R. *Science* **2008**, *321*, 833−836.

(11) Moosmüller, H.; Chakrabarty, R. K.; Ehlers, K. M.; Arnott, W. P. *Atmos. Chem. Phys.* **2011**, *11*, 1217−1225.

(12) Hecobian, A.; Zhang, X.; Zheng, M.; Frank, N.; Edgerton, E. S.; Weber, R. J. *Atmos. Chem. Phys. Discuss.* **2010**, *10*, 7601−7639.

(13) Chang, J.; Thompson, J. E. *Atmos. Environ.* **2010**, *44* (4), 541−551.

(14) Thompson, J. E.; Hayes, P. L.; Jimenez, J. L.; Adachi, K.; Zhang, X.; Liu, J.; Weber, R. J.; Buseck, P. R. *Atmos. Environ.* **2012**, *55*, 190−200.

(15) Gyawali, M.; Arnott, W. P.; Zaveri, R. A.; Song, C.; Moosmuller, H.; Liu, L.; Mishchenko, M. I.; Chen, L.-W. A.; Green, M. C.; Watson, J. G.; Chow, J. C. *Atmos. Chem. Phys.* **2012**, *12*, 2587−2601.

(16) Ajtai, T.; Filep, A.; Schnaiter, M.; Linke, C.; Vragel, M.; Bozoki, Z.; Szabo, G.; Leisner, T. *J. Aerosol Sci.* **2010**, *41*, 1020−1029.

(17) Thompson, J. E.; Barta, N.; Policarpio, D.; DuVall, R. *Optics Express* **2008**, *16* (3), 2191−2205.

(18) Dial, K. D.; Hiemstra, S. D.; Thompson, J. E. *Anal. Chem.* **2010**, *82*, 7885−7896.

(19) Bevington, P. R.; Robinson, D. K. *Data Reduction for the Physical Sciences*; McGraw-Hill: New York, 1992;, pp 41−50.

(20) Redmond, H.; Thompson, J. E. *Phys. Chem. Chem. Phys.* **2011**, *13*, 6872−6882.

(21) Toon, O. B.; Pollack, J. B.; Khare, B. N. *J. Geophys. Res.* **1976**, *81*, 5733−5748.

(22) Nakayama, T.; Matsumi, Y.; Sato, K.; Imamura, T; Yamazaki, A.; Uchiyama, A. *J. Geophys. Res.* **2010**, *115*, D24204.

(23) Dubovik, O.; Holben, B. N.; Kaufman, J.; Yamasoe, M.; Smimov, A.; Tan, D.; Slutsker, I. *J. Geophys. Res.* **1998**, *103* (D24), 31903−31923.

(24) Ma, L.; Zobeck, T. M.; Hsieh, D. H.; Holder, D.; Morgan, C. L. S.; Thompson, J. E. *Aeolian Res.* **2011**, *3* (2), 235−242.

(25) Redmond, H. E.; Dial, K. D.; Thompson, J. E. *Aeolian Res.* **2010**, *2*, 5−26.

(26) Linke, C.; Móhler, O.; Veres, A.; Mohácsi, A.; Bozóki, Z.; Szabó, G.; Schnaiter, M. *Atmos. Chem. Phys.* **2006**, *6*, 3315−3323.

(27) Zhang, X.; Lin, Y.-H.; Surratt, J. D.; Zotter, P.; Prevot, A. S. H.; Weber, R. J. *Geophys. Res. Lett.* **2011**, *38*, L21810.

(28) Jacobson, M. Z. *J. Geophys. Res.* **1999**, *104* (D3), 3527−3542.

(29) Ajtai, T.; Filep, A.; Utry, N.; Schnaiter, M.; Linke, C.; Bozoki, Z.; Szabo, G.; Leisner, T. J. *Atmos. Sci.* **2011**, *42*, 859−866.

(30) Arnott, W. P.; Moosmuller, H.; Rogers, C. F.; Jin, T.; Bruch, R. *Atmos. Environ.* **1999**, *33* (17), 2845−2852.